Toward Improving Microphysical Parameterizations of Conversion Processes

JERRY M. STRAKA

School of Meteorology, University of Oklahoma, Norman, Oklahoma

ERIK N. RASMUSSEN

National Severe Storms Laboratory, Norman, Oklahoma

(Manuscript received 21 September 1995, in final form 2 December 1996)

ABSTRACT

Prognostic equations are proposed for use in gridpoint models for the purpose of providing Lagrangian information without the need for computing Lagrangian trajectories. The information provided by the proposed methods might lead to improved representations of microphysical conversion processes. For example, the proposed methods could help improve the timing and location of the onset of precipitation in cloud models.

1. Introduction

We propose Eulerian form, prognostic equations to predict the Lagrangian age and displacement of parcels experiencing a condition or a physical process in gridpoint models. In addition, an Eulerian form, prognostic equation for the time-weighted mean of a variable, process, or condition is proposed as well. Our approach is novel in that Lagrangian information in an Eulerian gridpoint model is shown to be available without explicitly computing Lagrangian trajectories. We suggest that information available from these might be very useful for improving various parameterizations of microphysical processes in Eulerian models. While the methods we propose are exceedingly simple, they have not been used previously for improving microphysical parameterizations or for other purposes in meteorology, at least to our knowledge.

Most multidimensional, Eulerian cloud and mesoscale models incorporate various complex microphysical parameterization schemes to represent bulk hydrometeor characteristics and changes (e.g., Wisner et al. 1972; Koenig and Murray 1976; Cotton et al. 1982, 1986; Lin et al. 1983; Ferrier 1994). The Eulerian nature of these models has resulted in the use of microphysical parameterizations that depend on local gridpoint conditions. An unsolved problem in applying some of these parameterizations is that the conversion of one hydrometeor species to another typically does not commence, at least in the atmosphere, until a sufficient ''aging'' period has transpired given necessary conditions. By this we mean that there are some physical processes that must occur for certain periods of time before the conversion parameterizations representing these processes should be activated. Typically, though not always, this implies a nonlocal nature to the physical processes. Stated simply, microphysical parameterizations in Eulerian models fail to *explicitly* account for the Lagrangian history of the growth of cloud and precipitation particles.

An example of a microphysical process that depends on a certain ''aging'' period, given necessary conditions, is the transformation of cloud droplets to raindrop-sized hydrometeors (e.g., Cotton 1972; Cotton and Anthes 1989). The need to account for the relevant physics of this transformation in a simple manner for bulk microphysical models has resulted in the development of several autoconversion parameterizations (e.g., Berry 1968; Kessler 1969; Simpson and Wiggert 1969; Cotton 1972; Manton and Cotton 1977; Koenig and Murray 1976; Pruppacher and Klett 1981; Ziegler 1985). The physics represented by these parameterizations includes that diffusional growth produces a few droplets large enough to grow by collisional growth. The collisional growth rates of these larger drops increases with increasing drop size, which leads to the production of raindrops. The physical problem of autoconversion is complicated by the fact that diffusion tends to narrow cloud-drop distributions. A realistic autoconversion scheme needs to account for the physical processes that lead to distribution widening so that coalescence growth can become significant. Arguments have been made that larger droplets (i) might be produced as a result of isolated regions of higher super-

Corresponding author address: Dr. Jerry M. Straka, School of Meteorology, University of Oklahoma, Energy Center, 100 East Boyd St., Norman, OK 73019.
E-mail: jstraka@tornado.uoknor.edu

saturations that could promote rapid diffusional growth; (ii) might be provided from turbulent mixing of larger droplets from above; or (iii) could be provided by giant nuclei. Other arguments have implicated the importance of entrainment and successive small thermals. Cotton (1972), and Cotton and Anthes (1989) emphasized that *one* of the problems with autoconversion parameterizations developed thus far is that while some attempt to imply an implicit ''aging'' time for a droplet spectrum to widen sufficiently by diffusion and collisions to produce larger droplets, they all fail to *explicitly* account for the ''aging'' time required, among other factors,[1] for precipitation-sized particles to form. As a result many autoconversion schemes produce rainwater too soon and as a result too low in a cloud (e.g., Simpson and Wiggert 1969; Cotton 1972). Overly mature drops form assuming a constant drop distribution intercept or size can contribute to the problem. In an attempt to correct this problem, Cotton (1972) used a one-dimensional Lagrangian model to develop an autoconversion parameterization scheme that incorporated the age of a parcel with cloud drops in it. However, Cotton's autoconversion parameterization philosophy has not been used in his three-dimensional Eulerian cloud model (Manton and Cotton 1977; Cotton and Tripoli 1978; Tripoli and Cotton 1980; Cotton et al. 1982; Cotton et al. 1986; Flatau et al. 1989), or any other similar model known to the authors, because of computational cost and complexity in applying it in multidimensional Eulerian models. Tripoli and Cotton (1980) stated that a possible consequence of ignoring a time delay in an autoconversion scheme could make simulations of, for example, the weak-echo region in intense convective updrafts difficult if not impossible. As mentioned later, there are other similar problems with potentially important consequences when considering the ice phase.

The proposed methods are explained and developed in section 2 of this paper. Next, results using these methods in a simple idealized model and a three-dimensional cloud model are described in section 3. A summary, including a short discussion on the potential for the use of the proposed methods with other microphysical parameterizations, is provided in section 4.

2. Proposed method

There are a couple of ways to attempt to include Lagrangian information, such as age of a condition or physical process, in an Eulerian model. First, Lagrangian parcels could be released at every grid point and every time step as required for the duration of a simulation. While this sounds simple and effective, the memory and computational needs would be prohibitive, and the bookkeeping and remapping of all of the trajectories would be impractical. Alternatively, Lagrangian back-trajectories could be computed from each grid point at each time step, assuming a constant or steady-state time tendency. However, significant errors would be admitted owing to the nonsteady conditions that exist in most cloud systems.

To surmount the difficulties with the methods mentioned above, a simple means is sought for use in Eulerian models to predict the approximate Lagrangian ''age'' of a process or condition of parcels passing through grid points without explicitly computing Lagrangian trajectories. To explain the proposed method, suppose that the ''age'' τ of a condition in parcels is required, such as the time since cloud droplets are first produced in the parcel. Following the motion of the parcels, the age of the cloud parcel could be accumulated at each time interval when the mixing ratio of cloud droplets is nonzero or exceeds a specified threshold. The goal is to represent the essence of this aging process in an Eulerian model at each grid point where the condition is met.

Consider a prognostic equation for the age τ of a condition in parcels passing through grid points as a function of x, y, z, and t,

$$\frac{d\tau}{dt} = \frac{\partial \tau}{\partial t} + u\frac{\partial \tau}{\partial x} + v\frac{\partial \tau}{\partial y} + w\frac{\partial \tau}{\partial z} = c, \qquad (1)$$

where x, y, z, and t are the Cartesian coordinates and time, respectively; and c is either equal to 1 when the condition is met or 0 when it is not (c can be thought of as the Heaviside step function). When $c = 0$ (e.g., there is no cloud), τ could be set to 0 (age should be zero as the cloud has all evaporated), depending on the specific application. Integrating (1) from the initial times when the condition is first met gives the approximate ages of the condition of the parcels. As with Lagrangian trajectories, calculation and interpretation of Lagrangian information from (1) in flows with subgrid turbulence must be made with caution. Note that no information is provided by (1) concerning where parcels have been or where they originated, although the origin of parcels can be predicted by integrating equations for x, y, and z as is done for τ using (1) (discussed below). The proposed method predicts only the Lagrangian age of a condition associated with parcels as they pass through grid points, whereas in the Lagrangian framework the locations and conditions of parcels are predicted as a function of time following their motion.

Next, the x, y, and z displacement of parcels from where a physical condition or process first occurred or began also can be predicted in an Eulerian model by integrating the definition of velocity in an Eulerian framework:

[1] Factors that could be considered important in the transformation of cloud drops to raindrops include water content, droplet concentrations, distribution dispersion, aerosol concentrations, etc.

$$\frac{d\xi}{dt} = \frac{\partial \xi}{\partial t} + u\frac{\partial \xi}{\partial x} + v\frac{\partial \xi}{\partial y} + w\frac{\partial \xi}{\partial z} = uc$$

$$\frac{d\psi}{dt} = \frac{\partial \psi}{\partial t} + u\frac{\partial \psi}{\partial x} + v\frac{\partial \psi}{\partial y} + w\frac{\partial \psi}{\partial z} = vc$$

$$\frac{d\zeta}{dt} = \frac{\partial \zeta}{\partial t} + u\frac{\partial \zeta}{\partial x} + v\frac{\partial \zeta}{\partial y} + w\frac{\partial \zeta}{\partial z} = wc, \qquad (2)$$

where ξ, ψ, and ζ are the parcel displacements in the x, y, and z directions. As with (1), c can be thought of as acting as the Heaviside step function for the condition or process. The integration of these equations are discussed later to help show that the results from (1) are consistent with trajectory results.

Now, (1) can be used to derive a simple expression to predict, for example, the time-weighted mean of cloud water mixing ratio $\bar{q}_c$ that parcels have experienced as they pass through grid points. Information about $\bar{q}_c$ might be much more representative for indicating the potential for autoconversion rather than the value of cloud water mixing ratio at a grid point at a given time. Time weighted means of other variables or conditions also might be useful for other microphysical parameterizations. First, consider the definition of $\bar{q}_c$ following the motion in a Lagrangian parcel where τ is used as a bound on the integrals and τ' a dummy variable in the integration of $q_c(\tau')$:

$$\bar{q}_c = \frac{\int_0^\tau q_c(\tau')\, d\tau'}{\int_0^\tau d\tau'} = \frac{1}{\tau}\int_0^\tau \bar{q}_c(\tau')\, d\tau'. \qquad (3)$$

A prognostic equation for $\bar{q}_c$ in an Eulerian framework can be found by substitution of (3) into the total derivative for $\bar{q}_c$

$$\frac{d\bar{q}_c}{dt} = \frac{d}{dt}\left[\frac{1}{\tau}\int_0^\tau q_c(\tau')\, d\tau'\right] = \frac{d\tau}{dt}\frac{d}{d\tau}\left[\frac{1}{\tau}\int_0^\tau q_c(\tau')\, d\tau'\right]$$

$$= \frac{1}{\tau}q_c(\tau) - \frac{1}{\tau^2}\int_0^\tau q_c(\tau')\, d\tau' = \frac{q_c}{\tau} - \frac{\bar{q}_c}{\tau}, \qquad (4)$$

which permits

$$\frac{d\bar{q}_c}{dt} = \frac{\partial \bar{q}_c}{\partial t} + u\frac{\partial \bar{q}_c}{\partial x} + v\frac{\partial \bar{q}_c}{\partial y} + w\frac{\partial \bar{q}_c}{\partial z} = c\left(\frac{q_c}{\tau} - \frac{\bar{q}_c}{\tau}\right). \qquad (5)$$

The value $\partial\bar{q}_c/\partial t$ is the local time rate of change of $\bar{q}_c$ of the local rate of change of the time-averaged cloud water mixing ratio. Note the value $\partial\bar{q}_c/\partial t$ is not an average in the Eulerian sense but rather time weighted in Lagrangian viewpoint with regards to the value of τ, which is predicted.

Even though the behaviors of (1) and (5) are probably obvious, they are demonstrated, initially, using a very simple and idealized model. Assume a column of air with a vertical velocity w equal to 10 m s^{-1} at all of 10 levels, which are 100 m apart. Also assume that cloud water appears instantaneously at the initial time at levels 2–10, and the amounts remain constant in time. Solutions are obtained to (1) and (5) by using forward-in-time, upstream-in-space differences, and integrating them with a time step of 5 s for 150 s. The results at 5, 75, and 150 s are shown in Table 1. After one time step, the age is equal to the time step (5 s) at each level *in the cloud*, and the mean cloud content is equal to the actual cloud content as the cloud instantaneously appears at the initial time. After 150 s, the integration provides solutions that have converged to the exact solution. The behavior of (2), though not shown for this example, is similar in that the analytic solution is readily obtained.

TABLE 1. In this table, w (m s^{-1}) is vertical motion (constant in time), q_c is cloud content (constant in time), τ is the age of the condition that there is cloud in parcels as they pass through a grid point, and $\bar{q}_c$ is average cloud water mixing ratio that parcels have experienced as they pass through a grid point. The results below represent solutions to Eqs. (1) and (2).

Level	w	q_c	τ @ 5 s	τ @ 75 s	τ @ 150 s	$\bar{q}_c$ @ 5 s	$\bar{q}_c$ @ 75 s	$\bar{q}_c$ @ 150 s
10	10.0	9.0	5.0	72.7	90.0	9.0	5.6	4.5
9	10.0	8.0	5.0	69.6	80.0	8.0	4.7	4.0
8	10.0	7.0	5.0	64.6	70.0	7.0	3.9	3.5
7	10.0	6.0	5.0	57.7	60.0	6.0	3.2	3.0
6	10.0	5.0	5.0	59.2	50.0	5.0	2.6	2.5
5	10.0	4.0	5.0	39.8	40.0	4.0	2.0	2.0
4	10.0	3.0	5.0	30.0	30.0	3.0	1.5	1.5
3	10.0	2.0	5.0	20.0	20.0	2.0	1.0	1.0
2	10.0	1.0	5.0	10.0	10.0	1.0	0.5	0.5
1	10.0	0.0	0.0	0.0	0.0	0.0	0.0	0.0

3. Application and discussion

To further demonstrate the proposed method, one of the deep convective cloud simulations presented in Klemp and Wilhelmson (1978; hereafter KW78) are repeated. The simulation chosen assumes 10 m s^{-1} of shear in the u wind over a depth of 3 km in lower atmosphere. A spheroidal thermal perturbation placed in the center of the model domain at the initial time is used to initiate convection. These initial conditions result in a simulation of a storm that is symmetric about the center of the domain in the north–south direction. The three-dimensional cloud model used for the experiments described in this paper is briefly described in Straka and Anderson (1993). The model is set up to emulate the KW78 model. Included in the model are prognostic equations for the three momentum variables, potential temperature, pressure, turbulent kinetic energy, water vapor, and any number of other hydrometeor species. In addition, (1), (2), and (5) are included in the model to predict the age of the condition that cloud droplets are present in parcels, the displacement from where the condition is first met in parcels, and the mean cloud water content in parcels that pass through each grid point. The microphysical parameterization is similar to that described by KW78 and does

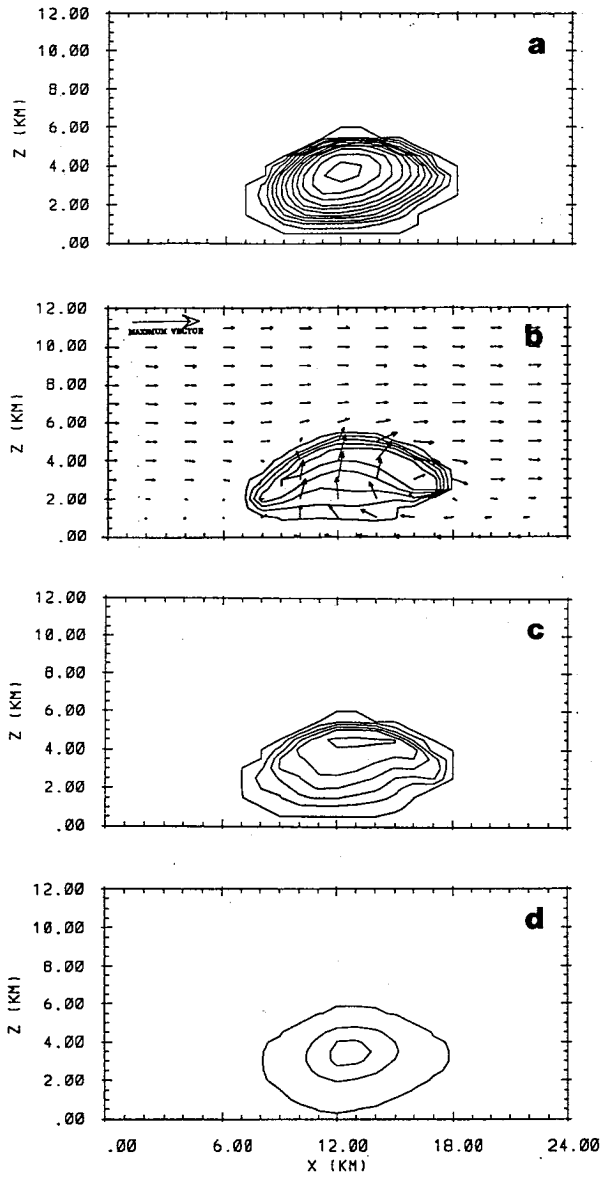

FIG. 1. Fields of (a) cloud mixing ratio q_c (contour interval of 0.25 g kg^{-1}); (b) cloud age τ (contour interval of 120 s starting at 60 s); (c) mean cloud mixing ratio $\bar{q}_c$ (contour interval of 0.25 g kg^{-1}); and (d) rain mixing ratio q_r (contour interval of 0.5 g kg^{-1}) in x–z cross sections through the center of the domain (y = 12 km) at 16 min. Wind vectors are included on the plot of cloud age. The large vector in the upper-left corner represents 30 m s^{-1}.

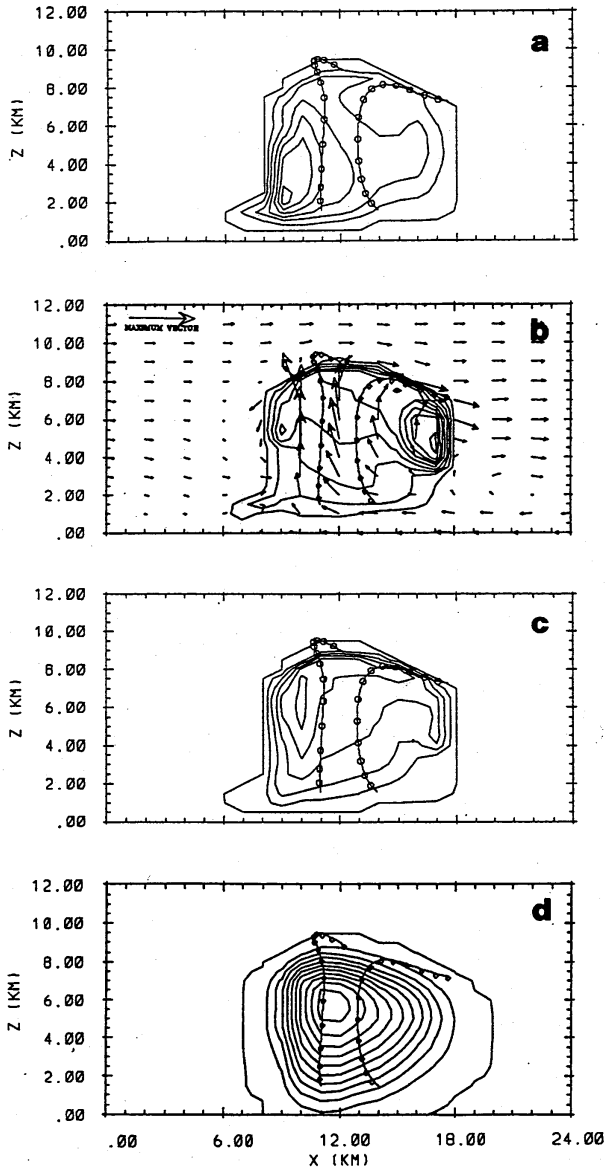

FIG. 2. Fields of (a) cloud mixing ratio q_c (contour interval of 0.25 g kg^{-1}); (b) cloud age τ (contour interval of 120 s starting at 60 s); (c) mean cloud mixing ratio $\bar{q}_c$ (contour interval of 0.25 g kg^{-1}); and (d) rain mixing ratio q_r (contour interval of 1.0 g kg^{-1}) in x–z cross sections through the center of the domain (y = 12 km) at 24 min. Wind vectors are included on the plot of cloud age. The traces of two trajectories, initiated at 960 s, also are indicated, with the circles indicating the trajectory positions every 60 s.

not consider ice processes. The source and sink terms include autoconversion of cloud water to rainwater, collection of cloud water by rainwater, and evaporation and vertical flux of rainwater. A saturation adjustment scheme accounts for the condensation and evaporation of cloud droplets.

Fields of cloud mixing ratio q_c, cloud age τ, mean cloud mixing ratio $\bar{q}_c$, and rain mixing ratio q_r in x–z cross sections through the center of the domain (y = 12 km) at 16 and 24 min are shown in Figs. 1 and 2, respectively. Velocity vectors are included on the plots of cloud age. The cloud water fields in Figs. 1a and 2a show maximum cloud contents in the regions where updrafts are a maximum. By 24 min, substantial amounts of the cloud water contents have been accreted by rain. At both times the values of cloud age, shown in Figs. 1b and 2b, are a minimum, not surprisingly, where updrafts are a maximum: τ increases from 0 at cloud base to 540 s surrounding the updraft summit. At 24 min, cloud ages

are greater than 540 s in a small region upwind (left) of the updraft and greater than 1000 s downwind (right) of the updraft in the upper-level outflow region. The maximum cloud age at 24 min is about 1050 s. The first cloud formed at about 300 s. The overall structure of the $\bar{q}_c$ fields shown in Figs. 1c and 2c appears similar to the q_c fields. At 16 min, amounts of $\bar{q}_c$ at any grid point typically are about 30%–60% of the amounts of q_c. However, by 24 min, maximum values of $\bar{q}_c$ are up to 75% of the largest values of q_c. And where rain has rapidly removed much cloud water by accretion, $\bar{q}_c$ can exceed q_c by small amounts for a short time. It should be noted that the autoconversion scheme used generally produces small amounts of rain. It is accretion that produces the larger amounts of rain, even at early times. However, cloud amounts to be accreted are small at early times.

An additional experiment was done using $\bar{q}_c$ instead of cloud water in the autoconversion parameterization. The results show some differences as should be expected. Some differences are that the mean cloud content above the autoconversion threshold (1 g kg^{-1}) is limited to the upper parts of the updraft Fig. 3. This is a direct result of larger cloud water contents owing to autoconversion being delayed. With higher cloud contents there are higher mean contents than the original run. The age of the parcels looks similar to the previous simulation. Finally, the rain has not reached as close to the ground compared to the other simulation.

The goal in this paper is not to develop an autoconversion scheme, only the necessary concepts so one can be built. However, an autoconversion scheme that uses results from integration of the stochastic equation, mean cloud content, and predicted age is being built. This scheme is in development and will be reported later.

The accuracies of (1), (2), and (5) are tentatively accessed by running many trajectories in real-time with the model integration (the trajectories are stepped forward during each time step of the Eulerian model integration). Two of the trajectories are shown on Fig. 2 from 16 to 28 min at 1-min intervals. Values of τ and $\bar{q}_c$ computed along the trajectories (assumed to be the truth values) and values of these variables produced by the integration of (1) and (5) in the model, at the trajectory locations, are compared in Fig. 4 for two of the trajectories. Similarly, the results of ξ and ζ from (2), the parcel displacements in the x and z directions, respectively, are shown in Fig. 5. The trajectories are initiated at 960 s along the center of the domain in the north–south direction, which is the axis of symmetry for the storm given the unidirectional shear and the location of the initial thermal perturbation. With no v wind component at the center of the domain in the north–south direction, the trajectories are confined to the x–z plane. The trajectory traces are shown in Figs. 2 and 3 as lines with small circles, which represent ''parcel'' locations every 60 s after initiation. A comparison of the ''ages'' predicted by (1) with the actual ages of the trajectories shows very good agreement with errors of less than 1%–2% as long as the trajectories are in the cloud and away from the cloud boundary. When the trajectories pass through the cloud boundary the errors increase dramatically as expected. This usually is not a problem as the important conversion physics generally occur well inside the cloud boundary. Nevertheless, caution must be taken in evaluating results near these boundaries. The mean cloud mixing ratios predicted by (5) also agree very well with the values along the trajectories (Fig. 4b). And as with (1), the errors with (5)

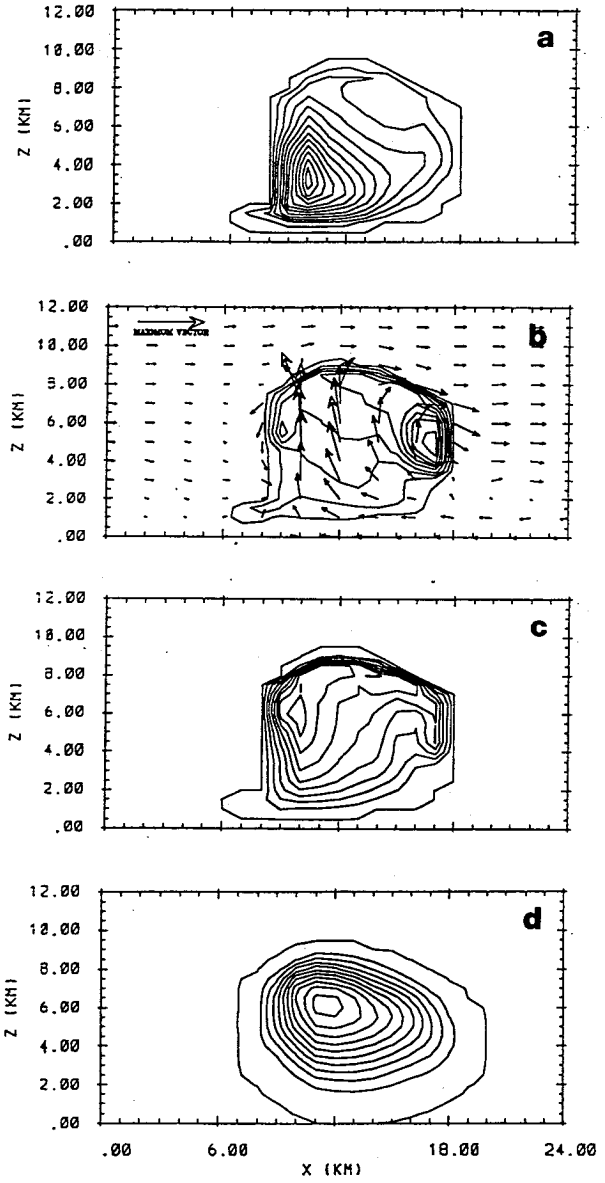

FIG. 3. Fields of (a) cloud mixing ratio q_c (contour interval of 0.25 g kg^{-1}); (b) cloud age τ (contour interval of 120 s starting at 60 s); (c) mean cloud mixing ratio $\bar{q}_c$ (contour interval of 0.25 g kg^{-1}); and (d) rain mixing ratio q_r (contour interval of 1.0 g kg^{-1}), in x–z cross sections through the center of the domain (y = 12 km) at 24 min in simulation with $\bar{q}_c$ used in the autoconversion parameterazation. Wind vectors are included on the plot of cloud age.

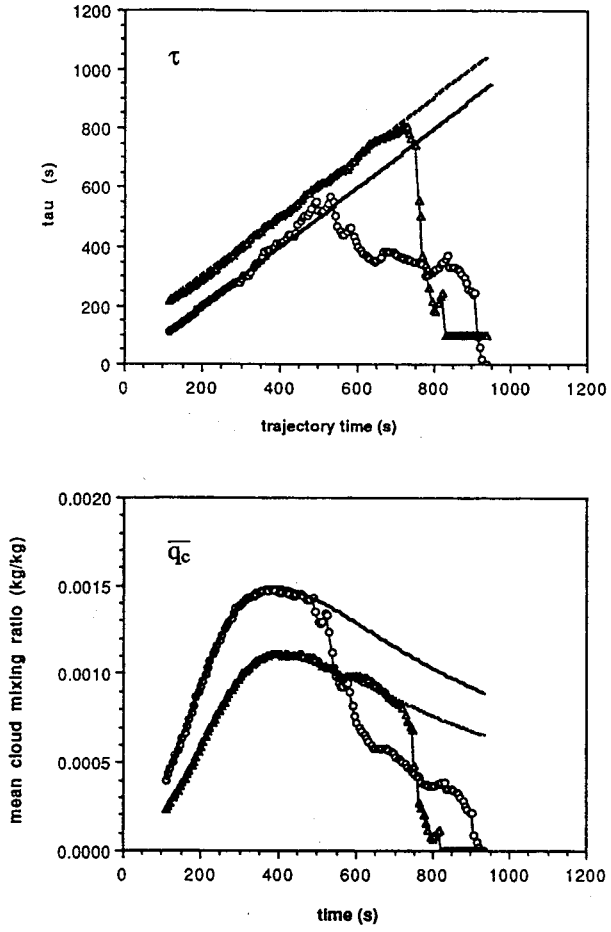

FIG. 4. Values of τ and $\bar{q}_c$ computed along the trajectories (solid and dashed bold lines; assumed to be the truth values) and values of these variables produced by integration of Eqs. (1) and (5) in the model (triangles and circles at each time step), at the trajectory locations for two trajectories. The bold dashed curve and circles correspond to the eastern trajectory, whereas the bold curve and triangles correspond to the western trajectory.

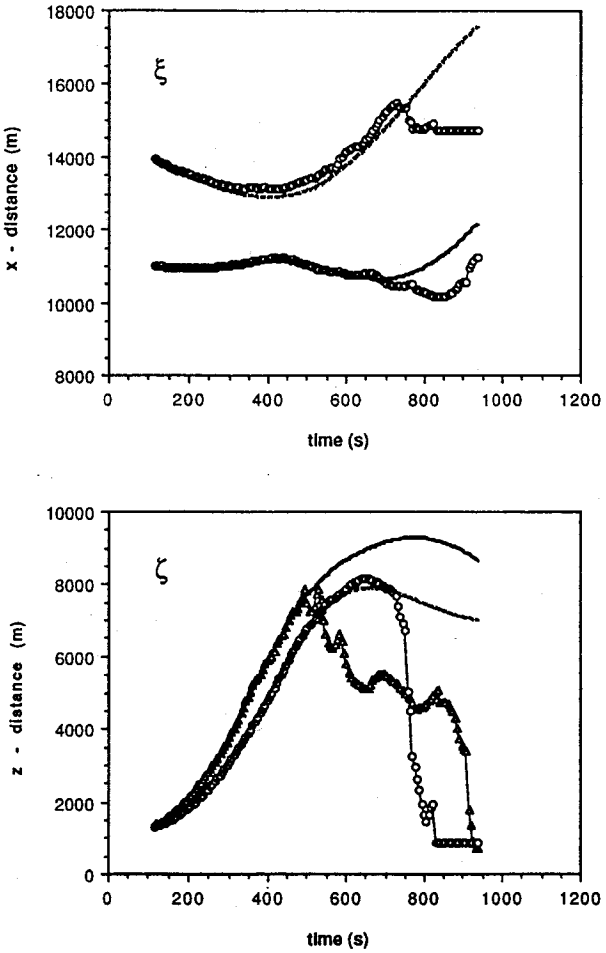

FIG. 5. Values of ξ and ζ computed along the trajectories (solid and dashed bold lines; assumed to be the truth values) and values of these variables produced by integration of Eq. (2) in the model (triangles and circles at each time step), at the trajectory locations for two trajectories. The bold dashed curve and circles correspond to the eastern trajectory, whereas the bold curve and triangles correspond to the western trajectory.

become very large as the trajectories pass through the boundaries. Finally, parcel displacements predicted with (2) versus the actual trajectory displacements are equally as good (Fig. 5). In addition, they suffer from similar boundary problems. The results from the integration of (2) help show that the results from (1) and (5) indeed are equivalent to integrating real trajectories. Other uses of (2) such as evaluating the origin of parcels in deep convective simulations might be possible (as suggested by Dr. R. Davies-Jones). However, these will not be discussed here as they are beyond the scope of this paper.

Next, the results of integrating (1) and (5) are put into context of where rain was formed in the model using the KW78 form of the microphysics parameterization. Note that rain is present (Fig. 1d) in the lowest regions of the updraft at 16 min (as well as at 24 min) where parcels of cloudy air are on the order of 60–180 s old, $q_c = 1$ to 1.5 g kg^{-1}, and $\bar{q}_c = 0.5$ to 1 g kg^{-1}. Careful examination of the source and sink terms for rain shows that this rain was produced by autoconversion (at least at 16 min): q_c is greater than the threshold of 1 g kg^{-1} for autoconversion with the Kessler scheme (KW78) (note the model's accretion parameterization has been activated). Of importance is whether rain should form there in less than 3 min. Assuming an initial cloud droplet radius of 2.5 μm[2] at cloud base, a number concentration of 200 cm^{-3}, and a mean steady-state supersaturation of 1.0075 [Eq. (9.10) in Young (1993): mean updraft of 6 m s^{-1} and a mean droplet size of 8 μm], integration of the diffusional growth equation [Eq. (5.12) in Young 1993] gives a droplet

[2] The results are not sensitive to initial droplets radii of 1–5 μm.

radius of 15 μm in 180 s and 19 μm in about 300 s. Even by assuming that a few larger droplets might be present (see footnote 1), sufficient collectional growth for autoconversion to occur probably would not be expected in 180 s, given that a nominal collector droplet radius of 19 μm is required for the initial collection of smaller droplets (see Cotton and Anthes 1989 and Young 1993 for reviews). Autoconversion thresholds could be modified so that autoconversion does not occur until there are larger amounts of cloud water at present at a grid point. But then the autoconversion scheme might prevent rain from forming where it should at some locations, even though the amounts are below the parameterization threshold. And, as we have mentioned, the parameterization still would not be general enough to account for the age of the processes that lead to autoconversion.

Before closing this section, a few words about implementing the proposed methods are provided. There are no subgrid turbulent mixing terms in the equations for age, displacement, and mean mixing ratio solutions. Therefore, a numerical filter or a monotonic advection scheme must be used to keep the solutions smooth enough for accurate advection. A sixth-order Crowley scheme with a monotonic adjustment worked well in preserving relatively sharp boundaries at the cloud edges in the simulations presented in this paper. A high-order filter also works well. However, significant errors within a grid point or two of the boundaries are unavoidable. In these regions ages and mean contents usually are too small and meaningless. Fortunately, many of the important conversion-type microphysics do not occur in these regions.

4. Summary

Prognostic equations for representing the time-averaged values of a quantity or age of a parcel have been proposed for use in gridpoint models. The information provided by these equations might be useful in improving parameterizations of the autoconversion of cloud droplets to rain. An aging problem also is present with parameterizations of the conversion of, for example, rimed ice crystals and aggregates to form graupel, and rimed graupel and frozen rain drops to form hail. It might be useful to know the time-weighted mean of the rime collected as well. In the detailed Ferrier (1994) microphysical parameterization, for example, a constant riming time of 120 s is used, and the rime density is dependent on local grid conditions. Preliminary model experiments using a scheme similar to Ferrier's suggest that graupel and hail production can be quite sensitive, in some situations, to the assumed riming time and local mean riming density. Improvements for these cloud auto conversion and other types of parameterizations will be reported in the near future.

Acknowledgments. We thank Drs. Robert P. Davies-Jones, Douglas K. Lilly, Alan Shapiro, Carl Hane, Ms. Yvette Richardson, and Ms. Kathy Kanak for their comments and encouragement. Special thanks are due to Shapiro for his mathematical assistance. In addition we are in debt to the reviewers for their extraordinary reviews; thank you.

REFERENCES

Berry, E. X., 1968: Comments on ''Cloud droplet coalescence: Statistical foundations and a one-dimensional sedimentation model.'' *J. Atmos. Sci.*, **25,** 151–152.

Cotton, W. R., 1972: Numerical simulation of precipitation development in supercooled cumuli—Part I. *Mon. Wea. Rev.,* **100,** 757–763.

——, and G. J. Tripoli, 1978: Cumulus convection in shear flow—three-dimensional numerical experiments. *J. Atmos. Sci.,* **35,** 1503–1521.

——, and R. A. Anthes, 1989: *Storm and Cloud Dynamics*. Academic Press, 883 pp.

——, M. A. Stephens, T. Nehrkorn, and G. J. Tripoli, 1982: The Colorado State University three-dimensional cloud model—1982. Part II: An ice phase parameterization. *J. Rech. Atmos.,* **16,** 295–320.

——, G. J. Tripoli, R. M. Rauber, and E. A. Mulvihill, 1986: Numerical simulation of the effects of varying ice crystal nucleation rates and aggregation processes on orographic snowfall. *J. Climate Appl. Meteor.,* **25,** 1658–1680.

Ferrier, B. S., 1994: A double-moment multiple-phase four-class bulk ice scheme. Part I: Description. *J. Atmos. Sci.,* **51,** 249–280.

Flatau, P. J., G. J. Tripoli, J. Verlinde, and W. R. Cotton, 1989: The CSU-RAMS cloud microphysical module: General theory and documentation. Technical Rep. 451, 88 pp. [Available from Dept. of Atmospheric Sciences, Colorado State University, Ft. Collins, CO 80523.]

Kessler, E., 1969: *On the Distribution and Continuity of Water Substance in Atmospheric Circulations. Meteor. Monogr.,* No. 32, Amer. Meteor. Soc., 84 pp.

Klemp, J. B., and R. B. Wilhelmson, 1978: The simulation of three-dimensional convective storm dynamics. *J. Atmos. Sci.,* **35,** 1070–1096.

Koenig, R., and F. W. Murray, 1976: Ice-bearing cumulus evolution: Numerical simulations and general comparison against observations. *J. Appl. Meteor.,* **15,** 742–762.

Lin, Y.L., R. D. Farley, and H. D. Orville, 1983: Bulk parameterization of the snow field in a cloud model. *J. Climate Appl. Meteor.,* **22,** 1065–1092.

Manton, M. J., and W. R. Cotton, 1977: Parameterization of the atmospheric surface layer. *J. Atmos. Sci.,* **34,** 331–334.

Pruppacher, H. R., and J. D. Klett, 1981: *Microphysics of Clouds and Precipitation.* D. Reidel Publishing, 714 pp.

Simpson, J., and V. Wiggert, 1969: Models of precipitating cumulus towers. *Mon. Wea. Rev.,* **97,** 471–489.

Straka, J. M., and J. R. Anderson, 1993: The numerical simulations of microburst producing thunderstorms: Some results from storms observed during the COHMEX experiment. *J. Atmos. Sci.,* **50,** 1329–1348.

Tripoli, G. J., and W. R. Cotton, 1980: A numerical investigation of several factors contributing to the observed variable intensity of deep convection over south Florida. *J. Appl. Meteor.,* **19,** 1037–1063.

Wisner, C. E., H. D. Orville, and C. G. Myers, 1972: a numerical model of a hail bearing cloud. *J. Atmos. Sci.,* **29,** 1160–1181.

Young, K. C., 1993: *Microphysical Processes in Clouds.* Oxford University Press, 427 pp.

Ziegler, C. L., 1985: Retrieval of thermal and microphysical variables in observed convective storms. Part I: Model development and preliminary testing. *J. Atmos. Sci.,* **42,** 1487–1509.